A new framework for analyzing structural volume changes of longitudinal brain MRI data

Bérengère Aubert-Broche, Vladimir Fonov, Daniel García-Lorenzo, Abderazzak Mouiha, Nicolas Guizard, Pierrick Coupé, Simon F. Eskildsen, Louis Collins

A New Framework for Analyzing Structural Volume Changes of Longitudinal Brain MRI Data

Berengere Aubert-Broche[1], Vladimir Fonov[1], Daniel García-Lorenzo[1,2], Abderazzak Mouiha[1], Nicolas Guizard[1], Pierrick Coupé[1,3], Simon Eskildsen[1,4], and D. Louis Collins[1]

[1] Montreal Neurological Institute, McGill University, Canada
[2] ICM, UPMC/INSERM UMR975 CNRS UMR7225, Hôpital de la Salpêtrière, Paris
[3] Laboratoire Bordelais de Recherche en Informatique, Unité Mixte de Recherche CNRS (UMR 5800), Bordeaux, France
[4] Aarhus University, Denmark

Abstract. Cross-sectional analysis of longitudinal MRI data might be sub-optimal as each dataset is analyzed independently. In this study, we evaluate how much variability can be reduced by analyzing structural volume changes of longitudinal data using longitudinal analysis. We propose a two-part pipeline that consists of longitudinal registration and longitudinal classification. The longitudinal registration step includes the creation of subject-specific linear and non-linear templates that are then registered to a population template. The longitudinal classification is composed of a 4D EM algorithm, using a priori classes computed by averaging the tissue classes of all time points obtained cross-sectionally.

To study the impact of these two steps, we apply the framework completely (called LL method: Longitudinal registration and Longitudinal classification) and partially (LC method: Longitudinal registration and Cross-sectional classification) and compare these to a standard cross-sectional framework (CC method: Cross-sectional registration and Cross-sectional classification).

The three methods are applied to (1) a scan-rescan database to analyze the reliability and to (2) the NIH pediatric population to compare the GM and WM growth trajectories, evaluated with a linear mixed-model. The LL method, and the LC method to a lesser extent, significantly reduce the variability in the measurements in the scan-rescan study and give the best fitted GM and WM growth models with the NIH pediatric database. The results confirm that both steps of the longitudinal framework reduce the variability and improve the accuracy compared to the cross-sectional framework, with longitudinal classification yielding the greatest impact.

1 Introduction

Longitudinal structural change measurements are crucial to study normal brain development and the impact on the brain growth of neurological disorders or neurodegenerative diseases.

S. Durrleman et al. (Eds.): STIA 2012, LNCS 7570, pp. 50–62, 2012.

While longitudinal MRI scans could be analyzed independently, recent methods propose to reduce intra-subject variability by taking into account longitudinal consistency whether for registration or tissue segmentation.

Longitudinal registration was first proposed by [15] by computing deformations between the longitudinal subject scans and a 4D template. Thereafter, methods using consistent diffeomorphic registration of longitudinal images were presented [7,12] and more recently, the creation of a subject-specific linear template was introduced [14].

Regarding longitudinal classification, a method has been proposed to incorporate longitudinal consistency constraints in a 3D fuzzy clustering segmentation [18]. In addition, 4D image segmentation was also presented with graph cuts algorithm [17].

Inspired by this previous work, we introduce a new method to measure structural volume changes in longitudinal MRI scans by using longitudinal information not only for registration but also for segmentation. First, we propose the creation of linear and non-linear subject-specific templates. Each time point is registered to the subject-specific template that is registered to the population template, making the registration of each timepoint to the population template more consistent. Second, we combine this registration with a 4D EM algorithm for tissue classification, using a priori classes computed by averaging the tissue classes of all time points obtained cross-sectionally to take advantage of the longitudinal consistency of the classification.

The method is applied to a scan-rescan database and to the NIH pediatric database to study the GM and WM volume growth in childhood. To evaluate the impact of the longitudinal registration and the longitudinal classification on the measurements, we compared this longitudinal analysis with a cross-sectional analysis and a hybrid analysis, using the longitudinal registration and a cross-sectional tissue classification.

2 Longitudinal Analysis Methods

The three methods to analyze longitudinal MRI data are as follows:

- method CC = Cross-sectional registration - Cross-sectional classification.

This is the standard pipeline. Each time point of each subject is analyzed independently. The registration steps explained in detail in the following section are performed without the linear and non-linear subject-specific template creation. Each time-point is directly registered to the population template. A standard [1] cross-sectional classification algorithm is employed.

- method LC = Longitudinal registration - Cross-sectional classification.

All the registration steps described below are applied, and then cross-sectional tissue classification algorithm [1] is used for each time point.

- method LL= Longitudinal registration - Longitudinal classification.

All the registration steps described below are applied and the longitudinal tissue classification is used. Figure 1 shows a flowchart with the steps involved in the LL method and the volume and registration notations used below.

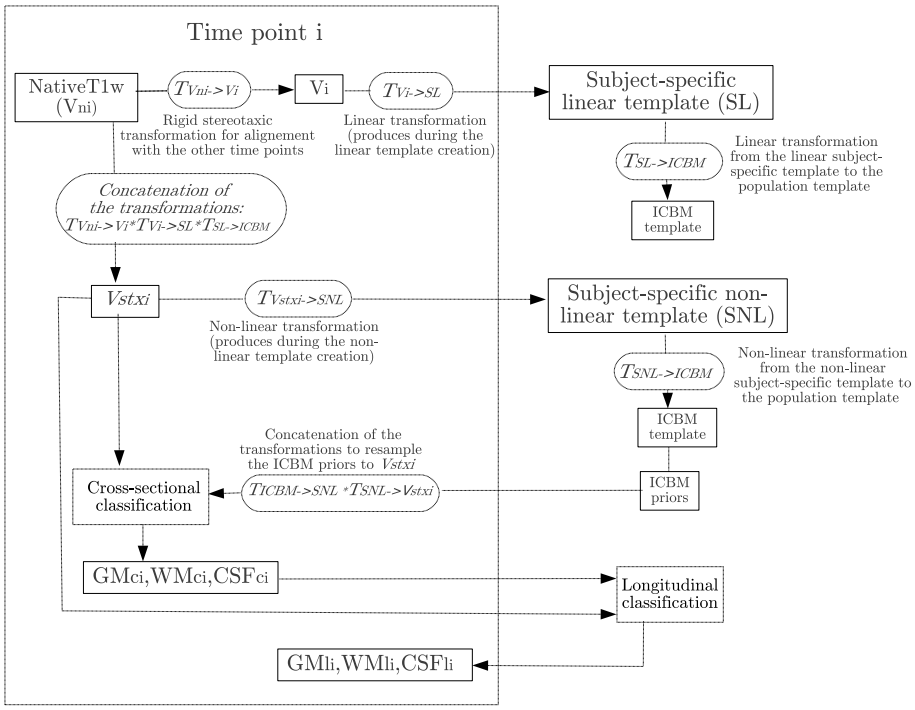

Fig. 1. Flow diagram of the LL method, for a time point i. (Vni: native T1w data of time point i, Vi: T1w data of time point i aligned with the other time points in the stereotaxic space but not scaled, Vstxi: T1w data of time point i linearly resampled in the stereotaxic space, GMci/WMci/CSFci: cross-sectional classification results for time point i, GMli/WMli/CSFli: longitudinal classification results for time point i, Tx->y, transformation from volume x to volume y, *: concatenation of transformations.

2.1 Registration Framework

Pre-processing. Three standard pre-processing steps were applied.

The first step following image reconstruction consists in removing noise in each MRI data by using the optimized non-local means filter [6]. The filtering parameter was set as the Rician noise standard deviation estimated using [5]. The second step corrects the impact of intensity inhomogeneity due to RF coil variations on MRI data using a non-parametric estimation of the slow varying non-uniformity field [16]. The third step scales the brain mean volume intensity to the target mean intensity (ICBM152 18.5-43.5 template) and linearly normalizes the intensity ranges to range 0-100 using histogram matching.

Linear Atlas Registration. A hierarchical nine-parameter linear registration based on intensity cross-correlation as a similarity measure is performed between each native T1w image (Vn_i) and the ICBM152 template [3].

Scale Removed Volume Alignment. All time points are aligned in the same stereotaxic space using only a rigid-body transformation, by removing scaling parameters calculated at the previous step. The resulting transformation for time point i is called $T_{V_{ni} \to V_i}$ in the Fig. 1 and the resulting volume is called V_i.

Iterative Subject-Specific Linear Template Creation. The subject template creation employs the principles of average template construction based on the work of [10]. A general diagram of the procedure for the jth iteration is shown in Fig. 2. For each iteration j ($j \in [1, 4]$) and for each time point i ($i \in [1, n]$), the algorithm is as follows:

- For each time point i, linear registration (a hierarchical twelve-parameter linear registration based on intensity cross-correlation) is performed, mapping $\mathrm{VTc}_{i,j-1}$ from the previous iteration to the current template SL_j, producing transformation $\mathrm{T}_{i,j}$. For the first iteration (j=1), $\mathrm{VTc}_{i,j-1}$ is V_i, the T1w volume of the time point i and SL_j is the T1w volume of the first time point (V_1).
- Average of all $\mathrm{T}_{i,j}$ transformations producing Ta_j.
- For each time point, concatenation of the transformation $\mathrm{T}_{i,j}$ with the inverse of the average transformation Ta_j ($\mathrm{Tc}_{i,j}$=$\mathrm{T}_{i,j}$*Ta_j^{-1}).
- Creation of $\mathrm{VTc}_{i,j}$, by resampling $\mathrm{V}_{i,j}$ using $\mathrm{Tc}_{i,j}$ transformation.
- Average of all $\mathrm{VTc}_{i,j}$ producing new subject template SL_{j+1}.

After this step we have a subject-specific linear template SL. For each time point, the resulting transformation from V_i to the subject-specific linear template SL is called $T_{V_i \to SL}$ in Fig. 1.

Subject-Specific Linear Template to Atlas Linear Registration. A hierarchical nine-parameter linear registration based on intensity cross-correlation as a similarity measure is performed between the subject-specific linear template (SL) and the ICBM152 template [3]. The resulting transformation is called $T_{SL \to ICBM}$ in Fig. 1.

T1 Resampling. Each native T1w volume (Vn_i) is only resampled once via the concatenated transformation: $T_{Vn_i \to Vi} * T_{Vi \to SL} * T_{SL \to ICBM}$ where * indicates the concatenation of transformations. The resulting resampled T1w volume (Vstx_i) is therefore in the ICBM152 template stereotaxic space.

Brain Segmentation. A multiresolution non-local segmentation technique is used to extract the brain in each resampled T1w volume (Vstx_i), using BEaST with a library of priors [8].

Iterative Subject-Specific Non-linear Template Creation. For each time point i and for each iteration j ($j \in [1, 12]$), the algorithm is as follows:

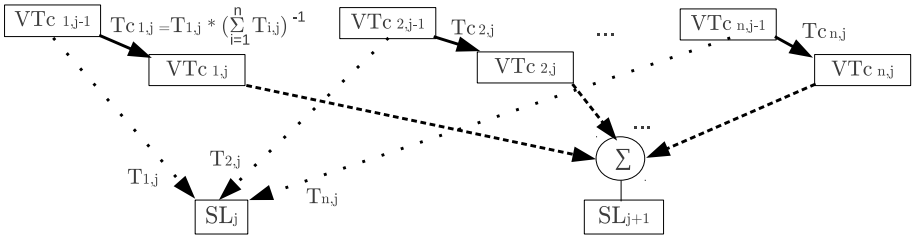

Fig. 2. Representation of the model creation algorithm for each iteration j: dotted lines represent the transformation from $\mathrm{VTc}_{i,j-1}$ (i, time point $\in [1...n]$) obtained in the previous iteration (or $\mathrm{V}_{i,j}$ for the first iteration) to the subject template SL_j (or the first time point volume V_1 for the first iteration), solid lines represent the creation of $\mathrm{VTc}_{i,j}$, by resampling $\mathrm{VTc}_{i,j-1}$ using $\mathrm{Tc}_{i,j}$ transformation, dashed lines represent the volumes averaged to compute the new subject template SL_{j+1}

- For each time point, non-linear registration ($\mathrm{T}_{i,j}$, a hierarchical non-linear registration based on intensity correlation coefficient, [2]) from $\mathrm{VTc}_{i,j-1}$ from the previous iteration to the current template SNL_j. For the first iteration (j=1), $\mathrm{VTc}_{i,j-1}$ is Vstx_i and SNL_j is the ICBM152 template.
- Average of all $\mathrm{T}_{i,j}$ transformations (Ta_j).
- For each time point, concatenation of the transformation $\mathrm{T}_{i,j}$ with the inverse of the average transformation Ta_j ($\mathrm{Tc}_{i,j}$=$\mathrm{T}_{i,j}$*Ta_j^{-1}).
- Creation of $\mathrm{VTc}_{i,j}$, the resampled $\mathrm{V}_{i,j}$ with $\mathrm{Tc}_{i,j}$ transformation.
- Average of all $\mathrm{VTc}_{i,j}$ to compute the new subject template SNL_{j+1}.

After this step we have a subject-specific non-linear template SNL. For each time point, the resulting transformation from Vstx_i to the subject-specific non-linear template SNL is called $T_{\mathrm{Vstx}_i \to SNL}$ in the Fig. 1.

Subject Non-linear Template to Atlas Non-linear Registration. A hierarchical non-linear registration based on intensity correlation-coefficient as a similarity measure is performed between the non-linear subject template and the ICBM152 template [2]. The resulting transformation is called $T_{SNL \to ICBM}$ in Fig. 1.

2.2 Classification

The classifications are performed on each T1w volume resampled in the template sterotaxic space (Vstx_i). For each voxel within the brain mask, a tissue label is assigned: grey matter(GM), white matter (WM) or cereobrospinal fluid (CSF).

Cross-Sectional Classification. For each time point, the label is assigned to each voxel using a two phase method [1]. First, a set of predefined standard tissue sample points in the stereotaxic ICBM152 template space is used to extract

intensity samples from the subject's MRI. A minimum-distance spanning tree is used to prune inconsistent samples, yielding a custom set of labels for the particular time point. Finally, this tag point set is used by an artificial neural network classifier to classify voxels in the brain.

Longitudinal Classification. A finite Gaussian mixture model is employed in the longitudinal classification. All time points T1w are merged in the same joint histogram. Expectation maximization (EM) is used to determine the parameters of the model [11]. The process is initialized by using *a priori* classes. For each tissue, an *a priori* class is computed by averaging the tissue classes of all the time points obtained in the cross-sectional classification and applying a 8 mm FWHM Gaussian filter.

2.3 Structure Segmentation

ICBM152 template region identification is merged with the output of the classification technique (GM, WM and CSF) in order to accurately identify specific structures [4]. These include frontal, temporal, occipital and parietal cortical GM and WM as well as internal structures (thalamus, putamen, globus pallidus and caudate).

2.4 Data

Two sets of data are used to evaluate the algorithm. First, a set of four scan-rescan datasets of T1w data from 20 young normal subjects is used (the 20NC-4V database). MRI data was acquired on a 1.5 T Siemens Sonata Vision clinical scanner (Siemens Medical Systems, Erlangen, Germany), using the standard head coil. Each subject was immobilised with a head restrainer. The protocol comprises four conventional whole-head high-resolution T1 scans. The T1-weighted scan was acquired using a 3D spoiled gradient echo (GRE) sequence ($TR = 22ms, TE = 9.2ms, \alpha = 30\,\mathrm{deg}$), providing whole head coverage with 1 mm isotropic voxel size. T1-weighted data were acquired on three different sessions within the same week (two in the first session, one in the second session and one in the fourth session).

The second database comes from the NIH-funded MRI study of normal brain development pediatric database (NIHPD) project that provides a database of normative pediatric MRI brain and behavioral data [9]. 882 multiple longitudinal MRI scans were obtained for 292 subjects aged 4.5-18.5 years at six pediatric study centers. Each subject had at least two scans, and at most four scans, with approximately two years between scans. The standardized MRI protocol included a whole brain, three-dimensional (3D) T1-weighted RF-spoiled gradient echo sequence with 1 mm thick sagittal partitions, TR= 22-25 ms, TE= 10-11 ms, excitation pulse angle 30 deg, 160-180mm FOV.

3 Results

3.1 Application to the 20NC-4V Database

Scan-rescan reliability was evaluated with the 20NC-4V database where no change between scans is expected. For each method k ($k = LL, LC, CC$) and for each subject j ($j = \{1...20\}$), we wanted to compare the size of the anatomical volumes computed from the four different acquisitions (Vi, $i = 1, 2, 3, 4$) ,where brain volumes were obtained with BEaST as described above, WM,GM and CSF obtained with the classifier and the anatomical structures were obtained using ANIMAL [4]. We compute the Volume Change (VC) defined as:

$$VC_{kji}(\%) = 100 * |1 - \frac{V_{kji}}{\frac{1}{4}\sum_{p=1}^{4} V_{kjp}}|$$

For each region and for each method k, a total volume change (tVC) is computed as follow:

$$tVC_k(\%) = \frac{1}{80}\sum_{j=1}^{20}\sum_{i=1}^{4} VC_{kji}$$

Fig. 3 shows the total volume changes for all regions and methods and Table 1 provides the mean and standard deviation (std) of the volume changes. For each region, the significance of the differences between each pair of methods (CC-LC, LC-LL and CC-LL) is given ($p<0.05$, Wilcoxon signed rank test).

If we compare the fourth column of Table 1 with the second and the third columns, it is clear that the volume differences estimated by the LL method are all smaller than the LC and CC volumes differences except for the globus pallidus region. The reduction is significant ($p<0.05$) in all regions except for the brain volume (Table 1, sixth and seventh columns). The brain volumes are the same between LL and LC methods as the two methods used the same framework, including the brain segmentation, up to the classification step. The differences between brain volumes estimated by the LL and CC methods are too small compared to the overall size of the brain to show significance. When we look at the second and the third columns, we can see that the volume changes are all smaller for the LC method than for the CC method, except for the CSF and the globus pallidus. However, the differences are significant only in the WM regions (Table 1, fifth column).

We can conclude that the LL method yields more stable results (smaller variability) with less bias (closer to zero, i.e., no change) than either the LC or CC methods. Furthermore, on average the LC method yields less biased results compared to the CC method.

3.2 Application to the NIHPD Database

For each subject and each time point, GM and WM volumes were estimated with the three methods. The GM and WM growth models were built using *nlme* package [13] in R. The maximum likelihood method was used to estimate model parameters.

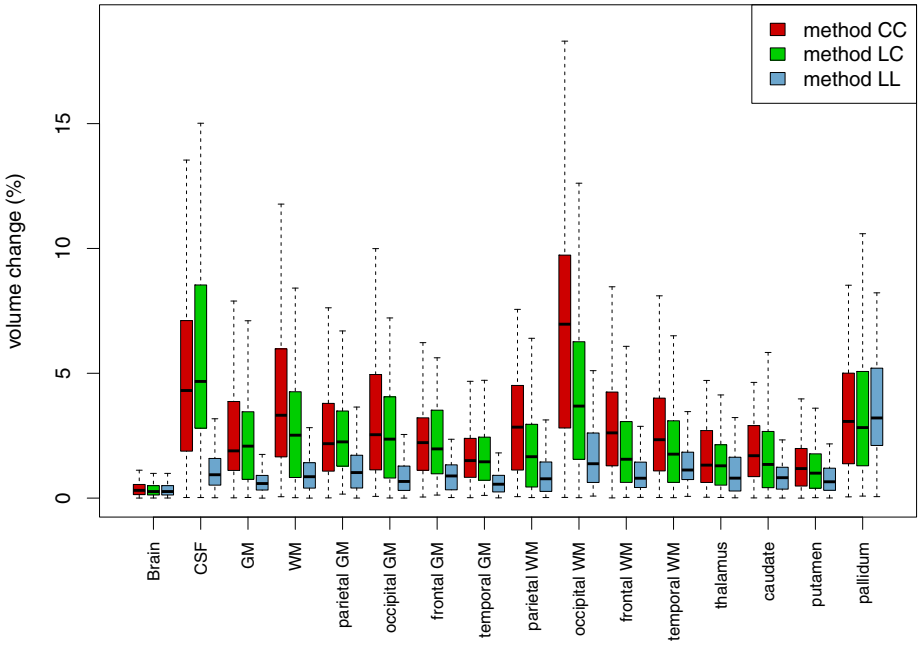

Fig. 3. Volume changes (in %) of structures segmentation on the scan-rescan 20NC-4V dataset, comparing the LL, LC and CC methods

Table 1. Volume changes (mean±std) averaged across subjects for the different anatomical structures for the scan-rescan 20NC-4V dataset. The * indicate the significantly reduced variability between CC and LC, LC and LL, and CC and LL methods.

Regions	CC method volume changes	LC method volume changes	LL method volume changes	CC-LC $p<0.05$	LC-LL $p<0.05$	CC-LL $p<0.05$
Brain	0.39 ± 0.38	0.36 ± 0.36	0.36 ± 0.36			
CSF	5.16 ± 4.17	5.87 ± 4.18	1.24 ± 1.03		*	*
GM	2.61 ± 2.15	2.32 ± 1.79	0.67 ± 0.51		*	*
WM	4.05 ± 3.07	2.86 ± 2.25	1.05 ± 0.85	*	*	*
parietal GM	2.69 ± 2.26	2.63 ± 1.89	1.31 ± 1.25		*	*
occipital GM	3.25 ± 2.43	2.61 ± 2.13	0.88 ± 0.81		*	*
frontal GM	2.42 ± 1.78	2.28 ± 1.64	0.99 ± 0.79		*	*
temporal GM	1.87 ± 1.46	1.75 ± 1.35	0.66 ± 0.53		*	*
parietal WM	3.08 ± 2.39	1.99 ± 1.69	1.02 ± 0.92	*	*	*
occipital WM	6.9 ± 4.57	4.27 ± 3.21	1.86 ± 1.67	*	*	*
frontal WM	2.98 ± 2.2	2.02 ± 1.63	0.99 ± 0.78	*	*	*
temporal WM	2.88 ± 2.42	2.11 ± 1.67	1.37 ± 0.91	*	*	*
thalamus	1.77 ± 1.42	1.46 ± 1.07	1.03 ± 0.82		*	*
caudate	1.94 ± 1.48	1.61 ± 1.3	0.9 ± 0.64		*	*
putamen	1.34 ± 1	1.18 ± 0.92	0.8 ± 0.61		*	*
pallidum	3.43 ± 2.42	3.45 ± 2.58	3.67 ± 2.3			

Table 2. Solution for fixed effects (Interc.: Intercept, DF:Degree of Freedom, Esti: Estimation, StEr: Standard Error, t: t-value) - WM and GM mean models for NIHPD population

		WM											
		LL method				LC method				CC method			
Effect	DF	Esti.	StEr	t	Pr>$\|t\|$	Esti.	StEr	t	Pr>$\|t\|$	Esti.	StEr	t	Pr>$\|t\|$
β_0(Interc.)	532	238.6	7.0	33.8	$<10^{-4}$	301.1	14.9	20.1	$<10^{-4}$	290.9	15.7	18.4	$<10^{-4}$
β_1(Age)	532	13.1	0.8	15.8	$<10^{-4}$	12.4	2.2	5.5	$<10^{-4}$	14.2	2.3	6.0	$<10^{-4}$
β_2(Age^2)	532	-0.19	0.03	-6.6	$<10^{-4}$	-0.23	0.08	-2.7	7.10^{-3}	-0.29	0.08	-3.4	7.10^{-4}
β_3(Sex)	338	9.5	7.5	1.2	0.20	20.5	12.3	1.6	0.09	24.4	13.1	1.8	0.06
β_4(Age*Sex)	532	2.6	0.4	5.7	$<10^{-4}$	2.3	0.9	2.3	0.02	2.1	1.0	2.1	0.03
		GM											
β_0(Interc.)	532	845.2	10.7	78. 4	$<10^{-4}$	795.5	18.35	43.3	$<10^{-4}$	799.6	18.97	42.14	$<10^{-4}$
β_1(Age)	532	7.04	1.4	5.0	$<10^{-4}$	5.98	2.73	2.1	0.02	4.52	2.83	1.59	0.11
β_2(Age^2)	532	-0.49	0.05	-9.5	$<10^{-4}$	-0.49	0.10	-4.9	$<10^{-4}$	-0.42	0.10	-4.04	10^{-4}
β_3(Sex)	338	77.48	6.7	11.4	$<10^{-4}$	71.89	6.88	10.4	$<10^{-4}$	70.44	6.97	10.10	$<10^{-4}$

Table 3. Criteria to compare the models fits - the smaller the AIC or BIC, the better the fit

	WM		
	LL method	LC method	CC method
Log Likelihood	-3851	-4500	-4556
AIC	7720	9018	9130
BIC	7763	9060	9173
	GM		
Log Likelihood	-4272	-4718	-4740
AIC	8559	9452	9497
BIC	8597	9490	9535

For each method, the following quadratic mixed model with fixed and random effects is defined as the best model for WM volumes using the Akaike's information criterion:

$$WM_{ij} = \beta_0 + \gamma_{0i} + (\beta_1 + \gamma_{1i}).Age + \beta_2.Age^2 + \beta_3.Sex_i + \beta_4.(Age * Sex)_i + \epsilon_{ij} \quad (1)$$

where

- WM_{ij} is the value of the WM volumes for the j time point of the subject i.
- β_0,...,β_4 are the fixed-effect coefficients which are identical for all subjects: β_0 is the intercept, β_1 the linear slope, β_2 the quadratic slope, β_3 the coefficient of sex (multiplied by 1 if male, 0 if female) and β_4 the interaction between age and sex.
- γ_{0i} and γ_{1i} are the random-effect coefficients for subject j, assumed to be mean 0 and constant variance. Because each subject has a different WM volume at the first time point, a random effect is added γ_{0i} to the intercept. Each subject has a different growth, so a random effect γ_{1i} is added to

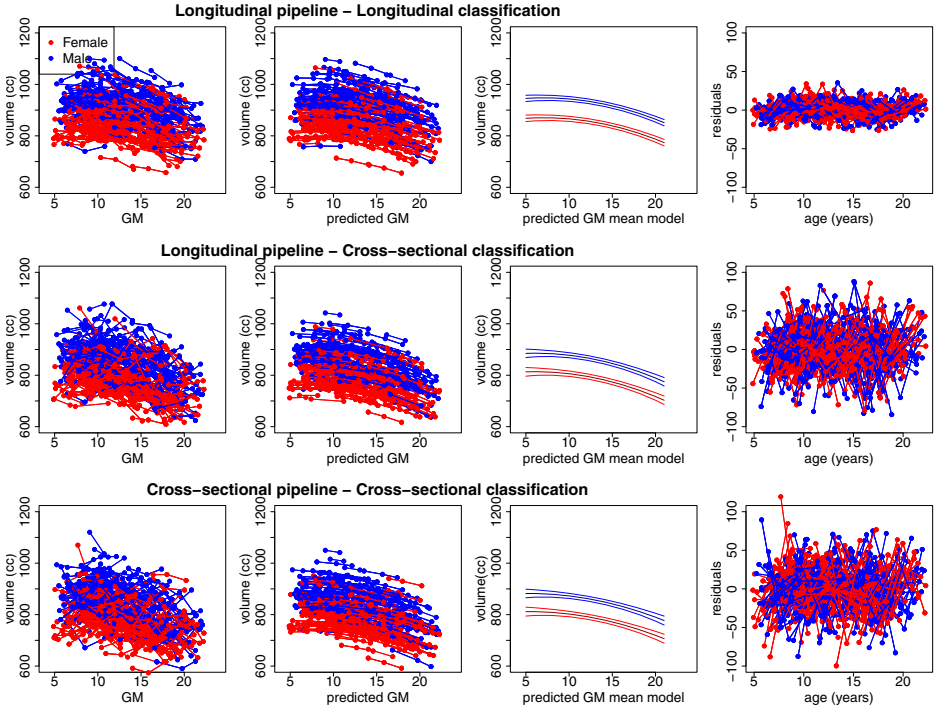

Fig. 4. Measured, predicted and GM volume mean model (with confidence intervals on the mean parameters) for the NIHPD population - From top to bottom: LL, LC and CC methods. Residuals are plotted in the rightmost column.

the linear slope. The variance-covariance matrix for the random effects is specified with a general symmetric positive-definite matrix.

– ϵ_{ij} is the error for time point j in subject i. The errors for group i are assumed to be mean 0 and constant variance and independent of the vector $(\gamma_{0i}, \gamma_{1i})$.

For GM volumes, the best-adjusted model is defined with the same fixed and random effects, except the age*sex interaction term that was not significant. The fixed effects estimated for each method are provided in Table 2. Table 3 gives information about the models fits. The Akaike's Information Criterion (AIC) and the Schwarz's Bayesian Information Criterion (BIC) are log-likelihood values adjusted for the number of parameters estimated in the model [13]. When comparing fitted models, the smaller the AIC or BIC, the better the fit.

From left to right, Fig. 4 and Fig. 5 display individual data points for measured GM and WM volumes respectively, individual data points for predicted GM and WM volumes, GM and WM mean model with confidence intervals and individual data points for residuals. For individual data points, longitudinal measurements from the same subject are connected by solid lines. The results of LL, LC and CC methods are respectively at the top, in the middle and at the bottom of Fig. 4 and Fig. 5.

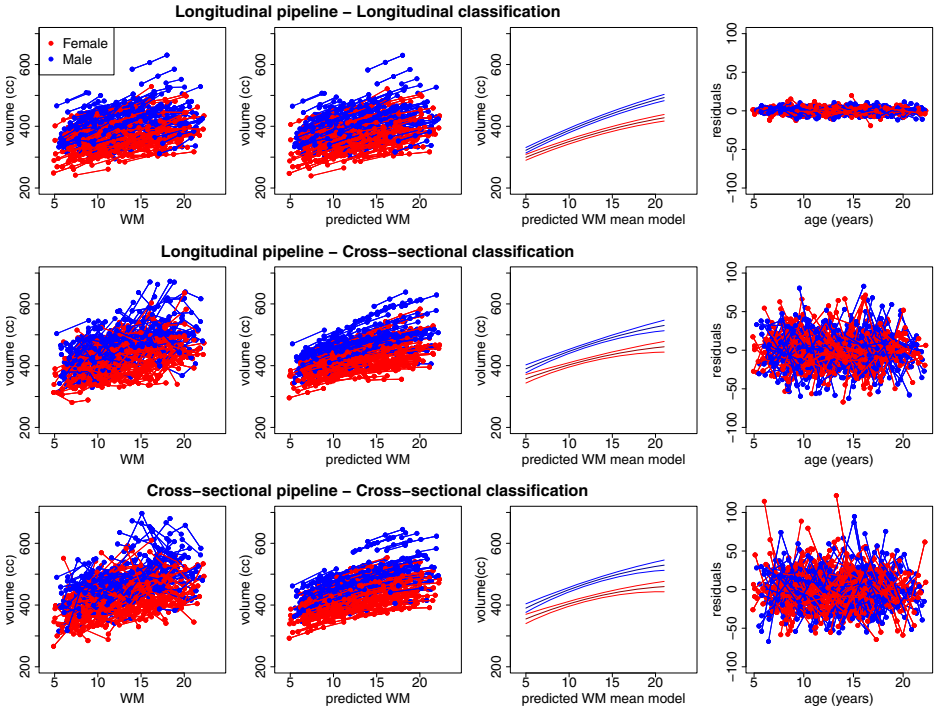

Fig. 5. Measured, predicted and mean model WM volumes (with confidence intervals on the mean parameters) for the NIHPD population - From top to bottom: LL, LC and CC methods. Residuals are plotted in the rightmost column.

We can clearly see on the graphs of Figs 4 and 5 that the standard deviation of the residuals, called the standard error of estimate (SEE), is smaller for the LL method than for the LC method and to a lesser extent, smaller for the LC method than for the CC method. The estimated fixed effects parameters are all more significant and the standard errors are all smaller for the LL method than for the other methods (cf Table 2), except for the sex effect in the GM growth model.

One should also note that due to the different algorithms used in the longitudinal and the cross-sectional classification, the WM/GM boundary is slightly shifted between the two classification results. That explains why the longitudinal classification obtains higher GM and lower WM volumes than the cross-sectional classification (cf Fig. 4 and 5).

4 Discussion and Conclusion

The scan-rescan experiments with the 20NC-4V data demonstrate that the LL pipeline has smaller variance and reduced bias in comparison to the LC and CC

pipelines. This indicates that the processing pipeline is stable and reduces noise associated with cross-sectional analysis by taking advantage of longitudinal consistency of the data. Moveover, the experiments with the NIHPD data indicate that LL pipeline is also sensitive to change and can be used to derive consistent parameters for a mixed model with fixed and random effects for analysis of growth trajectories. Using the NIHPD data, our results indicate that GM growth trajectory is driven by age, age^2 and sex effects, while WM is driven by age, age^2 and age$*$sex effects. These results will require further analysis and we will apply these techniques to individual structure growth trajectories in the future.

The reduced variance of the LL model enables the detection of subtle effects between groups. For example, in our analysis of the NIHPD data using the CC-method data, the age effect was not significant and the age^2 effect was less significant for GM while age^2 and sex effects were much less significant for WM. It is likely that with a smaller cohort, these effects would not have been detected with the CC pipeline. With the enhanced power of the LL pipeline due to reduced variance, smaller cohorts can be used to detect differences between groups. This is important in research studies where funds are limited and potentially useful in clinical trials to reduce cohort sizes or to reduce the time required for a trial.

Acknowledgements. Canadian Institutes of Health Research (MOP-111169 & 84360) and les Fonds de Recherche Santé Québec.

References

1. Cocosco, C.A., Zijdenbos, A., Evans, A.C.: A fully automatic and robust brain MRI tissue classification method. Med. Image Anal. 7(4), 513–527 (2003)
2. Collins, D.L., Evans, A.C.: ANIMAL: validation and applications of non-linear registration-based segmentation. Int. J. Pattern R. 11, 1271–1294 (1997)
3. Collins, D.L., Neelin, P., Peters, T.M., Evans, A.C.: Automatic 3D inter-subject registration of MR volumetric data in standardized Talairach space. J. Comput. Assist. Tomo. 18, 192–205 (1994)
4. Collins, D.L., Zijdenbos, A.P., Baaré, W.F.C., Evans, A.C.: ANIMAL+INSECT: Improved Cortical Structure Segmentation. In: Kuba, A., Sámal, M., Todd-Pokropek, A. (eds.) IPMI 1999. LNCS, vol. 1613, pp. 210–223. Springer, Heidelberg (1999)
5. Coupe, P., Manjon, J.V., Gedamu, E., Arnold, D., Robles, M., Collins, D.L.: Robust Rician Noise Estimation for MR Images. Med. Image Anal. 14(4), 483–493 (2010)
6. Coupe, P., Yger, P., Prima, S., Hellier, P., Kervrann, C., Barillot, C.: An optimized blockwise nonlocal means denoising filter for 3-d magnetic resonance images. IEEE Trans. Med. Imaging 27(4), 425–441 (2008)
7. Durrleman, S., Pennec, X., Trouvé, A., Gerig, G., Ayache, N.: Spatiotemporal Atlas Estimation for Developmental Delay Detection in Longitudinal Datasets. In: Yang, G.-Z., Hawkes, D., Rueckert, D., Noble, A., Taylor, C. (eds.) MICCAI 2009, Part I. LNCS, vol. 5761, pp. 297–304. Springer, Heidelberg (2009)
8. Eskildsen, S.F., Coup, P., Fonov, V., Manjn, J.V., Leung, K.K., Guizard, N., Wassef, S.N., Ostergaard, L.R., Collins, D.L.: BEaST: Brain extraction based on nonlocal segmentation technique. Neuroimage 59(3), 2362–2373 (2012)

9. AC Evans and Brain Development Cooperative Group. The NIH MRI Study of Normal Brain Development 30(1), 184–202 (2006)
10. Fonov, V., Evans, A., Botteron, K., McKinstry, R., Collins, D.: Unbiased average age-appropriate atlases for pediatric studies. Neuroimage 54(1), 313–327 (2011)
11. Garcia-Lorenzo, D., Prima, S., Arnold, D.L., Collins, D.L., Barillot, C.: Trimmed-likelihood estimation for focal lesions and tissue segmentation in multisequence MRI for multiple sclerosis. IEEE Trans. Med. Imaging 30(8), 1455–1467 (2011)
12. Lorenzi, M., Ayache, N., Frisoni, G., Pennec, X.: 4D registration of serial brain's MR images: a robust measure of changes applied to Alzheimer's disease. In: STIA, MICCAI (2010)
13. Pinheiro, J., Bates, D., DebRoy, S., Sarkar, D., R Core Team: nlme: Linear and nonlinear mixed effects models. R package version 3.1-104 (2012)
14. Reuter, M., Schmansky, N., Rosas, H., Fischl, B.: Within-subject template estimation for unbiased longitudinal image analysis. Neuroimage 61(4), 1402–1418 (2012)
15. Shen, D., Davatzikos, C.: Measuring temporal morphological changes robustly in brain MR images via 4-D template warping. Neuroimage 21(4), 1508–1517 (2004)
16. Sled, J.G., Zijdenbos, A.P., Evans, A.C.: A nonparametric method for automatic correction of intensity nonuniformity in MRI data. IEEE Trans. Med. Imaging 17(1), 87–97 (1998)
17. Wolz, R., Heckemann, R.A., Aljabar, P., Hajnal, J.V., Hammers, A., Lotjonen, J., Rueckert, D.: Measurement of hippocampal atrophy using 4D graph-cut segmentation: Application to ADNI. Neuroimage 52(1), 109–118 (2010)
18. Xue, Z., Shen, D., Davatzikos, C.: CLASSIC: consistent longitudinal alignment and segmentation for serial image computing. Neuroimage 30(2), 388–399 (2006)